

Strong enhancement of spin-orbit torques and perpendicular magnetic anisotropy in $[Pt_{0.75}Ti_{0.25}/Co–Ni\ multilayer/Ta]_n$ superlattices

Xiaomiao Yin(阴小苗), Zhengxiao Li(李政霄), Jun Kang(康俊), Changmin Xiong(熊昌民), and Lijun Zhu(朱礼军)

Citation: Chin. Phys. B, 2026, 35 (**1**): 018502. DOI: 10.1088/1674-1056/ae1c26
http://cpb.iphy.ac.cn; http://iopscience.iop.org/cpb

What follows is a list of articles you may be interested in

Interlayer exchange coupling effects on the spin-orbit torque in synthetic magnets

Haodong Fan(樊浩东), Zhongshu Feng(冯重舒), Tingwei Chen(陈亭伟), Xiaofeng Han(韩晓峰), Xinyu Shu(舒新愉), Mingzhang Wei(卫鸣璋), Shiqi Liu(刘士琦), Mengxi Wang(王梦溪), Shengru Chen(陈盛如), Xuejian Tang(唐学健), Menghao Jin(金蒙豪), Yungui Ma(马云贵), Bo Liu(刘波), and Tiejun Zhou(周铁军)

Chin. Phys. B, 2025, 34 (**9**): 098501. DOI: 10.1088/1674-1056/ade42c

Influence of exchange bias on spin torque ferromagnetic resonance for quantification of spin-orbit torque efficiency

Qian Zhao(赵乾), Tengfei Zhang(张腾飞), Bin He(何斌), Zimu Li(李子木), Senfu Zhang(张森富), Guoqiang Yu(于国强), Jianbo Wang(王建波), Qingfang Liu(刘青芳), and Jinwu Wei(魏晋武)

Chin. Phys. B, 2024, 33 (**5**): 058502. DOI: 10.1088/1674-1056/ad2d55

Ta thickness effect on field-free switching and spin-orbit torque efficiency in a ferromagnetically coupled Co/Ta/CoFeB trilayer

Zhongshu Feng(冯重舒), Changqiu Yu(于长秋), Haixia Huang(黄海侠), Haodong Fan(樊浩东),Mingzhang Wei(卫鸣璋), Birui Wu(吴必瑞), Menghao Jin(金蒙豪), Yanshan Zhuang(庄燕山),Ziji Shao(邵子雯), Hai Li(李海), Jiahong Wen(温嘉红), Jian Zhang(张鉴), Xuefeng Zhang(张雪峰),Ningning Wang(王宁宁), Sai Mu(穆赛), and Tiejun Zhou(周铁军)

Chin. Phys. B, 2023, 32 (**4**): 048504. DOI: 10.1088/1674-1056/aca7e9

RF magnetron sputtering induced the perpendicular magnetic anisotropy modification in Pt/Co based multilayers

Runze Li(李润泽), Yucai Li(李予才), Yu Sheng(盛宇), and Kaiyou Wang(王开友)

Chin. Phys. B, 2021, 30 (**2**): 028506. DOI: 10.1088/1674-1056/abcf9d

Perpendicular magnetization switching by large spin—orbit torques from sputtered Bi_2Te_3

Zhenyi Zheng(郑臻益), Yue Zhang(张悦), Daoqian Zhu(朱道乾), Kun Zhang(张昆), Xueqiang Feng(冯学强), Yu He(何宇), Lei Chen(陈磊), Zhizhong Zhang(张志仲), Dijun Liu(刘迪军), Youguang Zhang(张有光), Pedram Khalili Amiri, Weisheng Zhao(赵巍胜)

Chin. Phys. B, 2020, 29 (**7**): 078505. DOI: 10.1088/1674-1056/ab9439

RAPID COMMUNICATION

Strong enhancement of spin–orbit torques and perpendicular magnetic anisotropy in $[Pt_{0.75}Ti_{0.25}/Co–Ni\ multilayer/Ta]_n$ superlattices

Xiaomiao Yin(阴小苗)[1,2,3], Zhengxiao Li(李政霄)[2,4], Jun Kang(康俊)[1,3,†], Changmin Xiong(熊昌民)[3,5,‡], and Lijun Zhu(朱礼军)[2,4,§]

[1] *Beijing Computational Science Research Center, Beijing* 100193, *China*
[2] *State Key Laboratory of Semiconductor Physics and Chip Technologies, Institute of Semiconductors, Chinese Academy of Sciences, Beijing* 100083, *China*
[3] *Department of Physics, Beijing Normal University, Beijing* 100875, *China*
[4] *Center of Materials Science and Optoelectronics Engineering, University of Chinese Academy of Sciences, Beijing* 100049, *China*
[5] *Key Laboratory of Multiscale Spin Physics, Ministry of Education, Beijing Normal University, Beijing* 100875, *China*

(Received 17 September 2025; revised manuscript received 21 October 2025; accepted manuscript online 6 November 2025)

We report the development of the $[Pt_{0.75}Ti_{0.25}/Co–Ni\ multilayer/Ta]_n$ superlattice with strong spin–orbit torque, large perpendicular magnetic anisotropy, and remarkably low switching current density. We demonstrate that the efficiency of the spin–orbit torque increases nearly linearly with the repetition number n, which is in excellent agreement with the spin Hall effect of the $Pt_{0.75}Ti_{0.25}$ being essentially the only source of the observed spin–orbit torque. The perpendicular magnetic anisotropy field is also substantially enhanced by more than a factor of 2 as n increases from 1 to 6. The $[Pt_{0.75}Ti_{0.25}/Co–Ni\ multilayers/Ta]_n$ superlattice additionally exhibits deterministic, low-current-density magnetization switching despite the very large total layer thicknesses. The unique combination of strong spin–orbit torque, robust perpendicular magnetic anisotropy, low-current-density switching, and excellent high thermal stability makes the $[Pt_{0.75}Ti_{0.25}/Co–Ni\ multilayer/Ta]_n$ superlattice a highly compelling material candidate for ultrafast, energy-efficient, and long-data-retention spintronic technologies.

Keywords: spin–orbit torque, perpendicular magnetic anisotropy, spin Hall effect, magnetization switching

PACS: 85.75.–d, 72.25.Mk, 68.65.Cd, 96.12.Hg

DOI: 10.1088/1674-1056/ae1c26 **CSTR:** 32038.14.CPB.ae1c26

It has been a central topic to develop magnetic heterostructures that simultaneously exhibit strong perpendicular magnetic anisotropy, spin–orbit torques (SOTs), and efficient current-induced switching for spin-based memory, computing, and sensor technologies.[1–10] The efficiencies of the SOTs are directly related to the switching current and thus the overall energy efficiency of the devices in practical applications.[1,11,12] Meanwhile, the perpendicular magnetic anisotropy (PMA) critically determines the thermal stability and data retention of the nanodevices fabricated from these magnetic heterostructures. Reducing the device dimensions for high-density integration typically brings a beneficial reduction of the SOT switching current, but also a detrimental loss of thermal stability and data retention simultaneously.[2] Thus, the development of strategies that can simultaneously enhance both the PMA and the SOT is of great importance. Previous efforts over the past decade have established that SOTs can be significantly increased by moderately increasing the resistivity of a spin Hall metal via alloying[13–19] or atomic insertions,[20,21] or by stacking symmetry-broken spin–orbit superlattices.[22,23] However, there has been no previous report on spin–orbit superlattices that combine a strong spin Hall alloy with strong PMA.

In this work, we, for the first time, report the development of $[Pt_{0.75}Ti_{0.25}/Co–Ni\ multilayers/Ta]_n$ superlattices with enhanced SOTs, robust PMA, and low-current-density switching by combining the strong spin Hall alloy of $Pt_{0.75}Ti_{0.25}$[24] and the PMA Co–Ni multilayer. The Co–Ni multilayer is selected as the ferromagnetic layer since it has been suggested by previous experiments to have tunable PMA,[25–29] low magnetization, small magnetic damping,[30] ultrafast domain wall motion and switching dynamics,[31–35] and large tunnel magnetoresistance.[36]

As shown in Fig. 1(a), we sputter-deposited five spin–orbit superlattices of $[Pt_{0.75}Ti_{0.25}$ (2 nm)/Co–Ni multilayer/Ta (1.5 nm)$]_n$ with different repeat numbers n of 1, 3, 4, 5, and 6 on oxidized Si substrates at room temperature. For each repeat of the superlattice, the Co–Ni multilayer consists of

†Corresponding author. E-mail: jkang@csrc.ac.cn
‡Corresponding author. E-mail: cmxiong@bnu.edu.cn
§Corresponding author. E-mail: ljzhu@semi.ac.cn

© 2026 Chinese Physical Society and IOP Publishing Ltd. All rights, including for text and data mining, AI training, and similar technologies, are reserved.

$[Co(0.29\ nm)/Ni(0.36\ nm)]_3$ and functions as the spin current detector, whereas $Pt_{0.75}Ti_{0.25}$ serves as the spin current generator, while the 1.5 nm disordered Ta grown at a low rate of 0.0092 nm/s is selected following previous in-plane magnetized superlattice studies[23] to break the symmetry by blocking the spin current from the neighboring $Pt_{0.75}Ti_{0.25}$ layers from flowing into the Co–Ni multilayer underneath the Ta (Fig. 1(a)) but generates negligible spin current (Fig. 1(b)) likely due to its small thickness, very high resistivity,[13–23] and disordered structure caused by the low growth rate.[37] Note that, without the Ta symmetry-breaking layer, no SOTs would be expected in the Co–Ni multilayers because the spin currents from the two $Pt_{0.75}Ti_{0.25}$ layers below and above the Co–Ni multilayers would fully cancel out (Fig. 1(b)). The subscripts of $Pt_{0.75}Ti_{0.25}$ denote the volume percentages calibrated from the deposition rates of Pt and Ti. Each superlattice is seeded with 1 nm Ta for improved adhesion and is protected from oxidation by a top MgO (1.6 nm)/Ta (1.5 nm) bilayer, forming a total stack of Si/SiO_2/Ta (1 nm)/superlattice/MgO (1.6 nm)/Ta (1.5 nm). As shown in Fig. 1(c), the spin–orbit superlattices were patterned into $5 \times 60\ \mu m^2$ Hall bars by photolithography and argon ion etching, followed by the deposition of Ti (5 nm)/Pt (150 nm). All Hall bar devices were annealed at 250 °C for 1.5 hours under zero magnetic field in a vacuum of 1×10^{-9} Torr to enhance PMA. Annealing experiments reveal that the superlattice exhibits robust PMA and square hysteresis up to 400 °C, suggesting the high thermal stability of the $[Pt_{0.75}Ti_{0.25}$/Co–Ni multilayer/Ta$]_n$ superlattice. As a representative example, Fig. 1(d) shows the first harmonic Hall voltage hysteresis loops of $[Pt_{0.75}Ti_{0.25}$ (2 nm)/Co–Ni multilayer/Ta (1.5 nm)$]_6$ annealed at different temperatures for 1.5 hours. A control Co–Ni multilayer/Ta (1.5 nm) device confirms that current flowing through the 1.5 nm Ta cannot switch the adjacent Co–Ni multilayer due to negligible SOT (Fig. 1(e)).

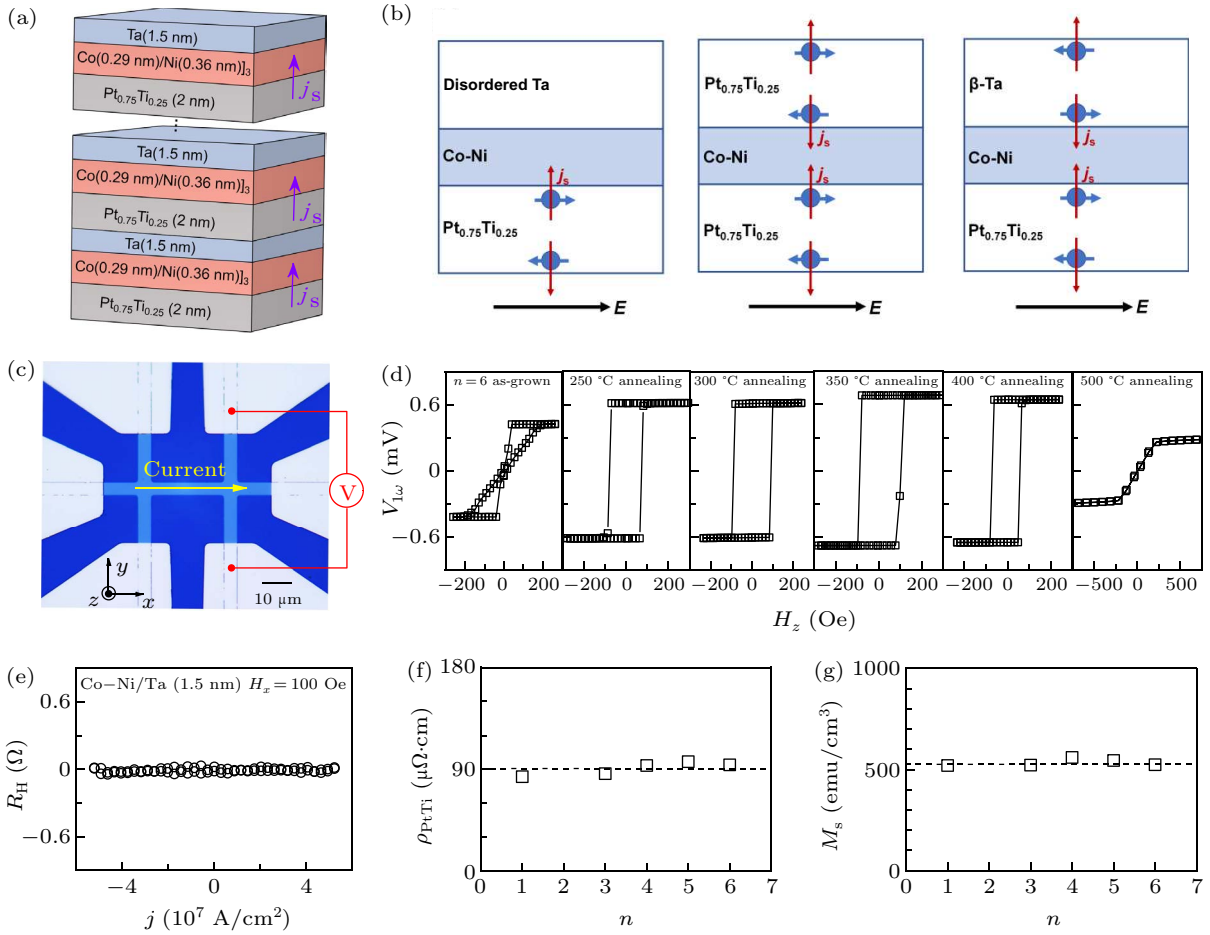


Fig. 1. Sample characteristics. (a) Schematic illustration of the $[Pt_{0.75}Ti_{0.25}$/Co–Ni multilayer/Ta$]_n$ superlattice. (b) Spin current configurations in disordered Ta/Co–Ni multilayer/$Pt_{0.75}Ti_{0.25}$, $Pt_{0.75}Ti_{0.25}$/Co–Ni multilayer/$Pt_{0.75}Ti_{0.25}$, and β-Ta/Co–Ni multilayer/$Pt_{0.75}Ti_{0.25}$. Spin currents from the under- and over-layers of the Co–Ni multilayer cancel out in $Pt_{0.75}Ti_{0.25}$/Co–Ni multilayer/$Pt_{0.75}Ti_{0.25}$, whereas they add constructively in β-Ta/Co–Ni multilayer/$Pt_{0.75}Ti_{0.25}$. In disordered Ta/Co–Ni multilayer/$Pt_{0.75}Ti_{0.25}$, the disordered Ta generates negligible spin current, leaving the top surface of $Pt_{0.75}Ti_{0.25}$ as the primary source of spin current injected into the Co–Ni multilayer. (c) Optical microscope image of the Hall bar device and the measurement configuration. (d) First harmonic Hall voltage versus perpendicular magnetic field for the $[Pt_{0.75}Ti_{0.25}$/Co–Ni multilayer/Ta$]_6$ in the as-grown state and after annealing for 1.5 hours at 250 °C, 300 °C, 350 °C, 400 °C, and 500 °C, respectively. (e) Hall resistance of the Co–Ni/Ta (1.5 nm) control device as a function of the average current density. (f) Average electrical resistivity of the $Pt_{0.75}Ti_{0.25}$ layers and (g) saturation magnetization (M_s) of the $[Pt_{0.75}Ti_{0.25}$/Co–Ni multilayer/Ta$]_n$ superlattices with different repeat numbers n.

As plotted in Fig. 1(f), the average resistivity of the $Pt_{0.75}Ti_{0.25}$ layers within the [$Pt_{0.75}Ti_{0.25}$ (2 nm)/Co–Ni multilayer/Ta (1.5 nm)]$_n$ superlattices is 91 ± 5 μΩ·cm, as estimated from the conductance enhancement of the Ta (1 nm)/[$Pt_{0.75}Ti_{0.25}$ (2 nm)/Co–Ni multilayer/Ta (1.5 nm)]$_n$/MgO (2 nm)/Ta (1.5 nm) stack relative to n times the conductance of a control stack without a $Pt_{0.75}Ti_{0.25}$ layer, i.e., Ta (1 nm)/Co–Ni multilayer/Ta (1.5 nm)/MgO (2 nm)/Ta (1.5 nm). The saturation magnetization (M_s) of each Co–Ni multilayer is 526 ± 20 emu/cm^3 as measured by a superconducting quantum interference device (Fig. 1(g) and the supplementary materials). These results suggest that the electrical and magnetic properties of each repeat of the [$Pt_{0.75}Ti_{0.25}$ (2 nm)/Co–Ni multilayer/Ta (1.5 nm)]$_n$ superlattices with $n \leq 6$ are essentially uniform and highly reproducible. Note that achieving such high-quality superlattices with n much greater than 6 remains challenging due to the gradual degradation of the structural identicalness of the repeated units.

The SOTs and PMA were characterized from the harmonic Hall voltages[14,38] under a sinusoidal electric field (E) of 33.3 kV/m applied along the x direction (Fig. 1(c)) in the low-field macrospin regime, explicitly taking into account thermoelectric effects.[39] To ensure reliable macrospin behavior and avoid potential multidomain artifacts, the samples were first saturated to the $+M_z$ ($-M_z$) state by applying a sufficiently large positive (negative) out-of-plane magnetic field (H_z). The in-phase first harmonic Hall voltage ($V_{1\omega}$) and the out-of-phase second harmonic Hall voltage ($V_{2\omega}$) were subsequently collected using a low-noise lock-in amplifier while sweeping the magnetic field along different directions in the low-field range. As representatively shown in Fig. 2(a), the superlattice samples exhibit well-defined and fairly square first harmonic Hall voltage hysteresis loops as a function of H_z, revealing the robust PMA of the superlattices. As shown in Fig. 2(b), $V_{1\omega}$ exhibits a parabolic dependence on the in-plane magnetic field, while $V_{2\omega}$ scales linearly with the in-plane magnetic field.

The square $V_{1\omega}$–H_z loops, the parabolic in-plane field dependence of $V_{1\omega}$, and the linear in-plane field dependence of $V_{2\omega}$ consistently indicate that the superlattices obey the macrospin model in the low-field regime,[1] which allows accurate and reliable estimation of the SOTs from the harmonic Hall voltage measurements. The dampinglike and fieldlike SOT effective fields, H_{DL} and H_{FL}, can be calculated as[39]

$$H_{DL} = -2\frac{\partial V_{2\omega}}{\partial H_x} \Big/ \frac{\partial^2 V_{1\omega}}{\partial^2 H_x} - 2H_k V_{ANE,z}/V_{AHE}, \quad (1)$$

$$H_{FL} = -2\frac{\partial V_{2\omega}}{\partial H_y} \Big/ \frac{\partial^2 V_{1\omega}}{\partial^2 H_y} - H_{Oe}, \quad (2)$$

where V_{AHE} is the anomalous Hall voltage extracted from the $V_{1\omega}$–H_z loops, H_k is the PMA effective field estimated from the parabolic in-plane dependence of $V_{1\omega}$ following $V_{1\omega} \approx V_{AHE}(1 - H_x^2/2H_k^2)$. H_{Oe} is the transverse Oersted field[30,31] generated in the Co–Ni multilayers by the in-plane charge currents in adjacent layers, and is calculated using the method described in Ref. [23]. The anomalous Nernst voltage, $V_{ANE,z}$, caused by an out-of-plane thermal gradient, can be measured directly from $V_{2\omega}$ when the magnetization is aligned along the x axis by applying a sufficiently large longitudinal field (Fig. 2(c)).

As summarized in Fig. 2(d), $V_{ANE,z}$ is negative and its magnitude increases systematically with the superlattice repetition number, consistent with prior reports on [Pt/Co/MgO]$_n$,[22] [PtCu/Co/Ta]$_n$,[23] and [Pt/Co/W]$_n$[40] superlattices. Microscopically, $V_{ANE,z}$ in a magnetic layer is determined by the product of the device width (fixed at 5 μm in this work) and the average electric field generated by the anomalous Nernst effect, $\boldsymbol{E}_{ANE} = S_{xy}\nabla \boldsymbol{T}_{FM} \times \boldsymbol{M}/|\boldsymbol{M}|$, where S_{xy}, $\nabla \boldsymbol{T}_{FM}$, and $\boldsymbol{M}$ represent the anomalous Nernst coefficient, the out-of-plane thermal gradient, and the magnetization vector, respectively. As illustrated schematically in the inset of Fig. 2(d), the out-of-plane thermal gradient arises naturally due to the different thermal dissipation at the top and bottom surfaces in contact with air and the substrate, respectively. Finite-element analysis[23] suggests that the observed increase of $V_{ANE,z}$ with n is primarily caused by a larger thermal gradient $\nabla \boldsymbol{T}_{FM}$ at increased total thickness, whereas S_{xy} remains essentially unchanged. Although S_{xy} has been reported to increase with interface density in some [Pt/Fe]$_n$ and [Pt/Ni]$_n$ multilayers,[41,42] the [$Pt_{0.75}Ti_{0.25}$/Co–Ni multilayer/Ta]$_n$ superlattices maintain identical interface density in each repeat, and thus S_{xy} is expected to remain effectively constant.

The significant anomalous Nernst voltage emphasizes the critical need to account for $V_{ANE,z}$ in harmonic Hall voltage analyses of SOTs in superlattices and multilayers, especially when $V_{ANE,z}$ is comparable to or even larger than the harmonic Hall voltage contributions of the SOTs. As demonstrated previously,[22] neglecting the strong anomalous Nernst effect, the dominant source of the second harmonic Hall voltage, can result in erroneously large estimates of the dampinglike SOT efficiency in multilayers such as effectively symmetry-preserved [Pt/Co]$_n$ with negligible actual SOTs. Experimentally, H_k is observed to increase substantially with the repetition number n from 1 to 6 (Fig. 2(e)), similar to [Pt/Co/MgO]$_n$,[22] likely due to enhanced interfacial spin–orbit coupling that is sensitive to atomic-scale interface details. This enhancement of H_k is highly beneficial for the development of nanoscale memory, computing, and sensor devices with improved thermal stability and long data retention times.

The efficiencies of the dampinglike SOT (ξ^j_{DL}) and fieldlike SOT (ξ^j_{FL}) are estimated as[43]

$$\xi^j_{DL(FL)} = \left(\frac{2e}{\hbar}\right)\mu_0 M_s t_{FM} H_{DL(FL)} \rho_{xx}/E, \quad (3)$$

where e is the elementary charge, $\hbar$ is the reduced Planck constant, μ_0 is the vacuum permeability, t_{FM} is the total magnetic layer thickness ($t_{FM} = 1.95n$ nm), and ρ_{xx} is the resistivity of the spin-current generator $Pt_{0.75}Ti_{0.25}$ (i.e., ρ_{PtTi} in Fig. 1(f)). As shown in Fig. 2(f), both ξ^j_{DL} and ξ^j_{FL} increase linearly with the repetition number n, i.e., $\xi^j_{DL} \approx 0.12n$ and $\xi^j_{FL} \approx 0.0025n$. This demonstrates that each repetition of the superlattice contributes nearly identical amounts to the dampinglike (0.12) and fieldlike (0.0025) SOTs. Since SOT efficiencies are defined per unit current density, the linear-in-n increase primarily arises from the increased total magnetic thickness, with only minor variations in H_{DL}, H_{FL}, or the spin Hall ratios of $Pt_{0.75}Ti_{0.25}$ during stacking. The smaller and opposite-sign fieldlike SOT and the linear-in-n trend confirm that the spin Hall effect is the dominant origin of SOTs in these symmetry-broken spin–orbit superlattices, with negligible collective stacking-induced contributions. These observations are consistent with previous results in in-plane anisotropy $[Pt_{0.75}Cu_{0.25}/Co/Ta]_n$ and PMA $[Pt/Co/W]_n$ superlattices[22,40] and with the absence of SOTs in symmetry-preserved $[Pt/Co]_n$ superlattices.[22]

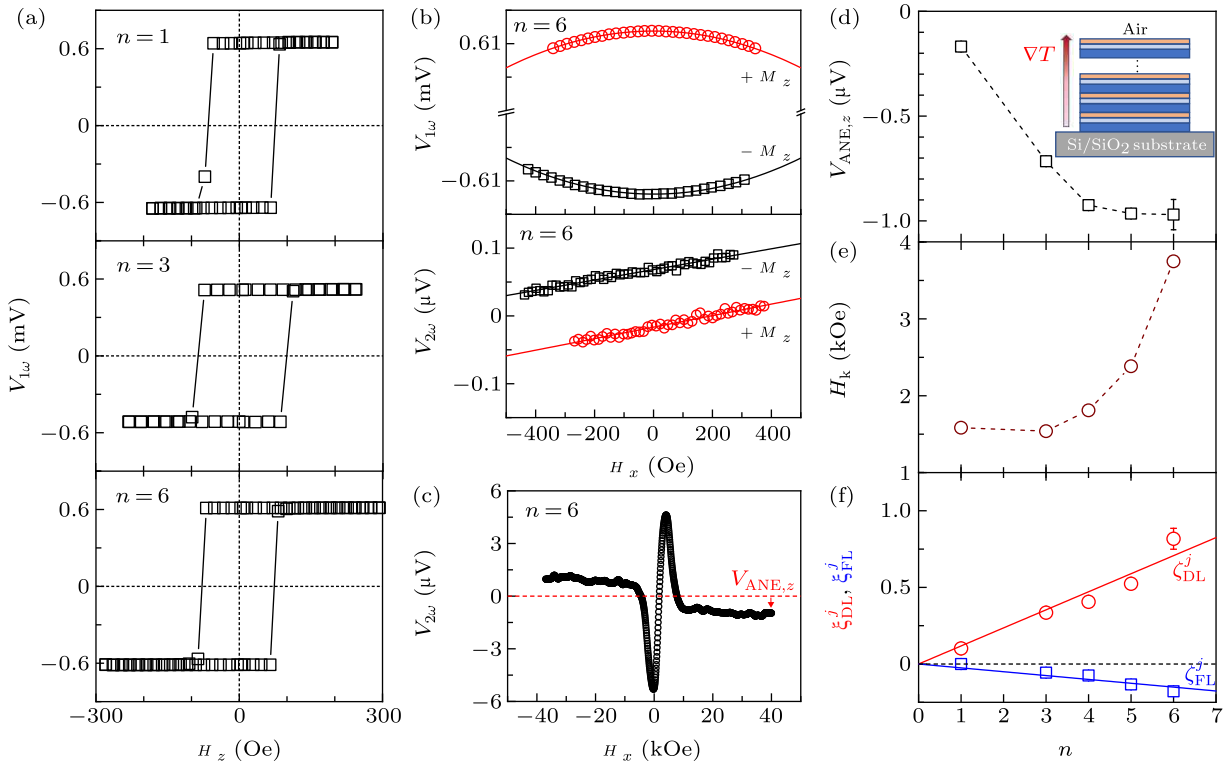


Fig. 2. Harmonic Hall voltage characterization of the $[Pt_{0.75}Ti_{0.25}/Co–Ni$ multilayer$/Ta]_n$ superlattices. (a) First harmonic Hall voltage ($V_{1\omega}$) as a function of the perpendicular magnetic field for the superlattices with $n = 1$, 3, and 6, demonstrating the evolution of the hysteresis with repetition number. (b) First ($V_{1\omega}$) and second ($V_{2\omega}$) harmonic Hall voltages plotted as a function of the in-plane field H_x for the superlattice with $n = 6$, highlighting the distinct parabolic and linear dependencies, respectively. (c) $V_{2\omega}$ versus H_x in the extended large field range, used for the precise determination of the anomalous Nernst voltage ($V_{ANE,z}$) for the superlattice with $n = 6$. Variation with n of (d) anomalous Nernst voltage ($V_{ANE,z}$), (e) perpendicular magnetic anisotropy field (H_k), and (f) dampinglike (ξ^j_{DL}) and fieldlike (ξ^j_{FL}) SOT efficiencies. The inset in panel (d) schematically illustrates the formation of the out-of-plane thermal gradient due to the distinct thermal dissipation rates at the top and bottom interfaces in contact with air and the substrate, respectively. The solid lines in panel (f) represent linear fits to the experimental data, emphasizing the systematic linear-in-n increase of the SOT efficiencies.

The spin Hall spin current responsible for the linear-in-n SOTs in $[Pt_{0.75}Ti_{0.25}/Co–Ni$ multilayer$/Ta]_n$ superlattice should be primarily attributed to the SHE of the $Pt_{0.75}Ti_{0.25}$, since experiments conducted by our group and other research groups[13–23] have consistently indicated negligible SOTs in Ta (1.5 nm)/FM bilayers. This negligible SOT is likely associated with the highly disordered structure of Ta resulting from the low sputter-deposition rate.[37] Notably, even β-phased Ta with a substantial thickness of 5 nm has been reported to generate a very small SOT efficiency of -0.01 in some $Ta/Ni_{81}Fe_{19}$ heterostructures,[44,45] let alone the highly disordered Ta with much smaller thickness and significantly weaker spin Hall effect. We also note that any nonzero spin current generated from the 1.5-nm Ta would contribute additively rather than subtractively to the spin current generated from the bottom $Pt_{0.75}Ti_{0.25}$ within the same superlattice repeat (Fig. 1(b)), because of the opposite signs of the spin Hall conductivities for Ta[2] and $Pt_{0.75}Ti_{0.25}$,[24] ultimately leading to further enhancement of the SOTs. We do not expect any additional torque contribution from the orbital Hall effect of Ta, as recent experiments have verified the absence of non-local orbital current torque in magnetic heterostructures containing both heavy metals[46–48] and light metals.[47–51] The linear-in-n scaling of ξ^j_{DL} also suggests that each 1.5 nm Ta symmetry-

breaking layer plays an ideal role in decoupling the spin currents of different superlattice repeats by effectively blocking the detrimental flow of spin current from the $Pt_{0.75}Ti_{0.25}$ overlayer within the neighboring repeat towards the Co–Ni multilayer within the same repeat of the Ta.

The ξ^j_{DL}/n value of 0.12 for the [$Pt_{0.75}Ti_{0.25}$/Co–Ni multilayer/Ta]$_n$ superlattice is smaller than that of the $Pt_{0.75}Ti_{0.25}$ (5.6 nm)/Fe (6 nm) bilayer reported in our previous work, which can be attributed to the relatively small thickness of the $Pt_{0.75}Ti_{0.25}$ layer in the superlattice and to the enhanced spin memory loss occurring at the $Pt_{0.75}Ti_{0.25}$/Co–Ni and Co/Ni interfaces. As discussed previously,[51] post-annealing can enhance the interfacial PMA as well as spin-memory loss via increased interfacial spin–orbit scattering of spins into the atomic lattice. However, we do not attribute the relatively low SOTs to any low-temperature thermal annealing-induced atomic intermixing, because atomic intermixing at the interfaces has been shown to reduce interfacial spin–orbit coupling and thus potentially enhance the SOTs by increasing the spin transparency of the HM/FM interfaces.[52]

The enhancement rate of the dampinglike SOT for the [$Pt_{0.75}Ti_{0.25}$/Co–Ni multilayer/Ta]$_n$ superlattice ($\xi^j_{DL}/n = 0.12$) is comparable to that of the in-plane anisotropy [$Pt_{0.75}Cu_{0.25}$/Co/Ta]$_n$ superlattices (0.13),[23] but smaller than that of the PMA [Pt/Co/W]$_n$ superlattices (0.173).[40] This difference can be attributed to the variations in spin Hall ratios, the thicknesses of the spin-current generators, and the interfacial spin memory loss.[51] The enhancement rate of the fieldlike torque (ξ^j_{FL}/n) is -0.025 for the [$Pt_{0.75}Ti_{0.25}$/Co–Ni multilayer/Ta]$_n$, which is distinct from those of the [$Pt_{0.75}Cu_{0.25}$/Co/Ta]$_n$ superlattices ($-0.017n$)[23] and the [Pt/Co/W]$_n$ superlattices (-0.027).[40] Different superlattice designs also exhibit different upper limits for the repeat number n (> 16 for [$Pt_{0.75}Cu_{0.25}$/Co/Ta]$_n$, 12 for [Pt/Co/W]$_n$, 6 for the [$Pt_{0.75}Ti_{0.25}$/Co–Ni/Ta]$_n$) due to variations in strain relaxation and accumulation across different material combinations. Considering the differences in ξ^j_{DL}/n, ξ^j_{FL}/n, and n, the highest achieved SOT efficiencies of the [$Pt_{0.75}Ti_{0.25}$/Co–Ni/Ta]$_n$ superlattice ($\xi^j_{DL} = 0.72$, $\xi^j_{FL} = -0.15$) are smaller than those of the [$Pt_{0.75}Cu_{0.25}$/Co/Ta]$_n$ ($\xi^j_{DL} = 2.1$, $\xi^j_{FL} = -0.27$) and [Pt/Co/W]$_n$ ($\xi^j_{DL} = 2.2$, $\xi^j_{FL} = -0.32$). Nevertheless, the linear-in-n enhancement of the SOT efficiencies is expected to persist for the [$Pt_{0.75}Ti_{0.25}$/Co–Ni multilayer/Ta]$_n$ superlattice with $n > 6$, provided that the degradation of PMA and repeat uniformity can be mitigated through further optimization of the growth protocols.

Finally, we demonstrate that the [$Pt_{0.75}Ti_{0.25}$/Co–Ni multilayer/Ta]$_n$ superlattices, despite their large magnetic layer thickness of up to 11.7 nm, can be efficiently switched by current-induced SOTs under an in-plane assisting magnetic field (H_x). As schematically illustrated in Fig. 3(a), during the current switching measurement, short square current pulses of 67 μs duration (j_{pulse1}) were applied to the superlattice Hall-bar devices as the write current using a Keithley 6221 source. To read the Hall resistance of the device after each write pulse, a long, low-magnitude read current pulse (j_{pulse2}) of 1 s duration and 0.1 mA amplitude was applied to the Hall-bar device with a 3-second delay relative to the write pulse, using another Keithley 6221 as the read excitation. The separation of write and read currents minimizes the influence of Joule heating on the measured Hall voltage and resistance. The current switching hysteresis loops of the superlattices with different n ($H_x = 100$ Oe) are shown in Fig. 3(b). As summarized in Fig. 3(c), the switching current averaged from the upward and downward transitions $(j_{c,\uparrow} - j_{c,\downarrow})/2$ remains approximately constant for the superlattices with different repeat numbers n, reflecting the high uniformity of the superlattice repeats despite the increase in magnetic layer thickness. The switching current density of the [$Pt_{0.75}Ti_{0.25}$/Co–Ni multilayer/Ta]$_n$ superlattices exhibits no simple scaling with H_k (Fig. 2(e)), consistent with the well-established observation that the switching of PMA devices is predominantly governed by anti-domain nucleation rather than macrospin coherent rotation.[53,54] As reported recently in Refs. [53,54], the current density required for anti-domain nucleation is collectively influenced by a variety of factors, including the SOT efficiencies, the Dzyaloshinskii–Moriya interaction (DMI), the in-plane magnetic field, the magnetic anisotropy, the pinning field, and others. The switching current is positively correlated with H_k but negatively with the DMI. Since the increase of H_k likely indicates an enhancement of interfacial SOC and consequently the DMI,[55,56] the overall effects of enhanced PMA and DMI may effectively cancel each other in terms of their influence on the current density. As shown in Fig. 3(d), the critical current densities for the upward ($j_{c,\uparrow}$) and downward ($j_{c,\downarrow}$) switching exhibit only a weak dependence on the in-plane magnetic field, in agreement with previous reports on Co-based PMA systems (see Fig. S1 in Ref. [12] for Pt-X/Co bilayer data and Ref. [40] for [Pt/Co/W]$_n$ superlattices).

While the switching current density of 1.5×10^7 A/m^2 falls within the range typically observed for switching only 1 nm thick three dimensional (3D) ferromagnetic layers in conventional heavy metal/ferromagnet bilayers,[14–19] we emphasize that current-driven switching of such thick magnetic layers is highly unexpected in the conventional bilayer scheme. In these systems, a 3D magnetic layer of several nanometers, or even as thick as 11.7 nm, is generally unlikely to be switchable by interfacial SOT before device failure occurs. The demonstrated ability of the superlattice to effectively switch a large-volume magnetic layer is particularly promising for spintronic applications in which the magnetic layer must be sufficiently thick to maintain robust PMA and/or thermal stability when the lateral dimensions are scaled down to tens of nanometers.

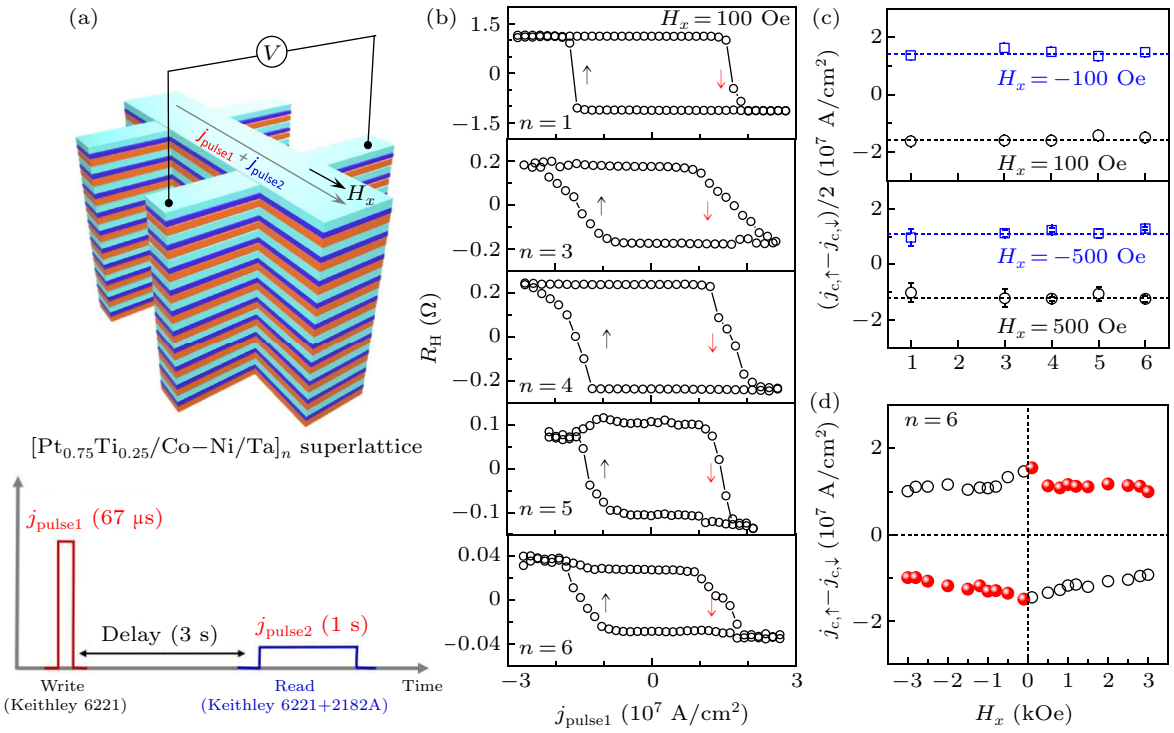


Fig. 3. Current switching of the $[Pt_{0.75}Ti_{0.25}$ (2 nm)/Co–Ni multilayer/Ta (1.5 nm)$]_n$ superlattices. (a) Schematic of the measurement configuration for current switching (see the main text for detailed discussion). (b) Hall resistance vs the average current density (j_{pulse1}) for the superlattice devices with different n under a longitudinal magnetic field of $H_x = 100$ Oe, with the black and red arrows indicating the upward and downward switching. (c) Dependence on n of the average switching current density, $(j_{c,\uparrow} - j_{c,\downarrow})/2$, for the superlattice devices under in-plane magnetic field of $H_x = \pm 100$ Oe and $H_x = \pm 500$ Oe. (d) Dependence on H_x of the upward and downward switching current densities ($j_{c,\uparrow}$ and $j_{c,\downarrow}$) for the superlattice device with $n = 6$.

Since the power consumption scales with $(1/\xi_{DL}^{j})^2$, such superlattices should exhibit approximately n^2 times lower power consumption to generate a given spin torque compared to a conventional magnetic bilayer of equivalent total magnetic thickness. These superlattices can therefore be employed to develop self-torqued magnetic tunnel junctions and superlattice racetracks for memory, computing, and microwave emitter applications that require low power, long operational endurance, low impedance, and large magnetic volume for enhanced thermal stability or improved signal output. It is noteworthy that the switching current density is not symmetric for upward and downward switching in the $n = 1$ sample (Fig. 3(d)), which, as discussed in detail in Refs. [56,57], can likely be attributed to antisymmetric anti-domain nucleation or a chiral perpendicular magnetic field arising from the DMI and magnetic non-uniformity.

We also note that the current switching results in Fig. 3(b) indicate Hall resistance variations corresponding to 100%, 78%, 78%, 74%, and 50% of the H_z-driven switching for the superlattices with $n = 1, 3, 4, 5$, and 6, respectively. The reduced switching ratio in the thick, large-n superlattice devices is likely due to partial switching. Similar partial current-induced switching under in-plane magnetic fields has been widely observed in various ferromagnetic and ferrimagnetic PMA systems.[58–64] While the exact mechanism of partial switching remains not fully understood, we anticipate that the switching will become increasingly complete as the device dimensions are reduced toward the practical scale of a few tens of nanometers, resulting in more uniform devices. We also emphasize that the switching current density associated with partial switching in the $[Pt_{0.75}Ti_{0.25}$/Co–Ni multilayer/Ta$]_n$ superlattices remains an important parameter for potential applications, as such switching is highly repeatable and deterministic. Partial switching can thus also be technologically useful. Notably, even the switching of small skyrmions within an unswitched magnetic host has been shown to be electrically detectable via magnetic tunnel junction resistance measurements.[65]

In summary, we have developed the $[Pt_{0.75}Ti_{0.25}$/Co–Ni multilayer/Ta$]_n$ superlattice with strong spin–orbit torque, robust perpendicular magnetic anisotropy, efficient current-induced switching, and high thermal stability. We demonstrate that the efficiency of the spin–orbit torque increases linearly with the repetition number n, which is in excellent agreement with the spin Hall effect being the dominant source of the torque. Meanwhile, the perpendicular magnetic anisotropy field is also enhanced by more than a factor of 2 as n increases from 1 to 6. The large-thickness $[Pt_{0.75}Ti_{0.25}$/Co–Ni multilayer/Ta$]_n$ superlattice can also be patterned into very thin nanopillars following the method of Watanabe *et al.*,[66] achieving strong perpendicular shape magnetic anisotropy and thereby considerably enhanced thermal stability and data retention. Furthermore, the superlattice exhibits deterministic magnetization switching despite the very large layer

thicknesses at relatively low current densities. The combination of strong spin–orbit torque, robust perpendicular magnetic anisotropy, low impedance, low-current switching, and high thermal stability renders the $[Pt_{0.75}Ti_{0.25}/Co–Ni$ multilayer$/Ta]_n$ superlattice a highly promising candidate for ultrafast, energy-efficient, and long-data-retention spintronic memory and logic technologies.

Acknowledgments

This project was supported by the Beijing Natural Science Foundation (Grant No. Z230006), the National Key Research and Development Program of China (Grant No. 2022YFA1204000), and the National Natural Science Foundation of China (Grant Nos. 12274405 and 12393831).

References

[1] Zhu L J 2023 *Adv. Mater.* **35** 2300853
[2] Liu L Q, Pai C F, Li Y, Tseng H W, Ralph D C and Buhrman R A 2012 *Science* **336** 555
[3] Miron I M, Garello K, Gaudin G, Zermatten P J, Costache M V, Auffret S, Bandiera S, Rodmacq B, Schuhl A and Gambardella P 2011 *Nature (London)* **476** 189
[4] Luo Z C, Hrabec A, Dao T P, Sala G, Finizio S, Feng J X, Mayr S, Raabe J, Gambardella P and Heyderman L J 2020 *Nature* **579** 214
[5] Zhang Y, Xu H J, Jia K, *et al.* 2023 *Sci. Adv.* **9** adg9819
[6] Hu S, Shao D F, Yang H L, Pan C, Fu Z X, Tang M, Yang Y M, Fan W J, Zhou S M, Tsymbal E Y and Qiu X P 2022 *Nat. Commun.* **13** 4447
[7] Liu L, Zhou C H, Zhao T Y, *et al.* 2022 *Nat. Commun.* **13** 3539
[8] Liang S X, Chen A T, Han L, Bai H, Chen C, Huang L, Ma M Y, Pan F, Zhang X X and Song C 2024 *Adv. Funct. Mater.* **35** 2417731
[9] Fan Y B, Wang Q, Wang W, Wang D, Huang Q K, Wang Z X, Han X, Chen Y X, Bai L H, Yan S S and Tian Y F 2024 *ACS Nano* **18** 26350
[10] Li R F, Zhang S, Luo S J, Guo Z, Xu Y, Ouyang J, Song M, Zou Q M, Xi L, Yang X F, Hong J M and You L 2021 *Nat. Electron.* **4** 179
[11] Lee O J, Liu L Q, Pai C F, Li Y, Tseng H W, Gowtham P G, Park J P, Ralph D C and Buhrman R A 2014 *Phys. Rev. B* **89** 024418
[12] Zhu L J, Ralph D C and Buhrman R A 2021 *Phys. Rev. Appl.* **15** 024059
[13] Zhu L J, Ralph D C and Buhrman R A 2021 *Appl. Phys. Rev.* **8** 031308
[14] Zhu L J, Ralph D C and Buhrman R A 2018 *Phys. Rev. Appl.* **10** 031001
[15] Zhu L J, Zhu L, Sui M L, Ralph D C and Buhrman R A 2019 *Sci. Adv.* **5** eaav8025
[16] Zhu L J, Sobotkiewich K, Ma X, Li X Q, Ralph D C and Buhrman R A 2019 *Adv. Funct. Mater.* **29** 1805822
[17] Hu C Y and Pai C F 2020 *Adv. Quantum Technol.* **3** 2000024
[18] Liu Q B, Li J W, Zhu L J, Lin X, Xie X Y and Zhu L J 2022 *Phys. Rev. Appl.* **18** 054079
[19] Quan J Z, Zhao X T, Liu W, Liu L, Song Y H, Li Y, Ma J, Li S Q, Zhao X G and Zhang Z D 2020 *Appl. Phys. Lett.* **117** 222405
[20] Zhu L J, Zhu L J, Shi S J, Sui M L, Ralph D C and Buhrman R A 2019 *Phys. Rev. Appl.* **11** 061004
[21] Zhu L J and Buhrman R A 2019 *Phys. Rev. Appl.* **12** 051002
[22] Zhu L J, Li J W, Zhu L J and Xie X Y 2022 *Phys. Rev. Appl.* **18** 064052
[23] Lin X, Zhu L J, Liu Q B and Zhu L J 2023 *Nano Lett.* **23** 9420
[24] Zhu L J and Ralph D C 2023 *Nat. Commun.* **14** 1778
[25] Seki T, Shimada J, Iihama S, Tsujikawa M, Koganezawa T, Shioda A, Tashiro T, Zhou W, Mizukami S, Shirai M and Takanashi K 2017 *J. Phys. Soc. Jpn.* **86** 074710
[26] Fukami S, Sato H, Yamanouchi M, Ikeda S and Ohno H 2013 *Appl. Phys. Express* **6** 073010
[27] Daalderop G H O, Kelly P J and den Broeder F J A 1992 *Phys. Rev. Lett.* **68** 682
[28] You L, Sousa R C, Bandiera S, Rodmacq B and Dieny B 2012 *Appl. Phys. Lett.* **100** 172411
[29] Mohanta M, Parida S K, Sahoo A, Hussain Z, Gupta M, Reddy V R and Medicherla V R R 2019 *Phys. B Condens. Matter* **572** 105
[30] Girod S, Gottwald M, Andrieu S, Mangin S, McCord J, Fullerton E E, Beaujour J M L, Krishnatreya B J and Kent A D 2009 *Appl. Phys. Lett.* **94** 262504
[31] Beaujour J M L, Chen W, Krycka K, Kao C C, Sun J Z and Kent A D 2007 *Eur. Phys. J. B* **59** 475
[32] Mangin S, Ravelosona D, Katine J A, Carey M J, Terris B D and Fullerton E E 2006 *Nat. Mater.* **5** 210
[33] Bedau D, Liu H, Bouzaglou J J, Kent A D, Sun J Z, Katine J A, Fullerton E E and Mangin S 2010 *Appl. Phys. Lett.* **96** 022514
[34] Koyama T, Yamada G, Tanigawa H, Kasai S, Ohshima N, Fukami S, Ishiwata N, Nakatani Y and Ono T 2008 *Appl. Phys. Exp.* **1** 101303
[35] Koyama T, Chiba D, Ueda K, Kondou K, Tanigawa H, Fukami S, Suzuki T, Ohshima N, Ishiwata N, Nakatani Y, Kobayashi K and Ono T 2011 *Nat. Mater.* **10** 194
[36] Moriyama T, Gudmundsen T J, Huang P Y, Liu L, Muller D A, Ralph D C and Buhrman R A 2010 *Appl. Phys. Lett.* **97** 072513
[37] Bansal R, Behera N, Kumar A and Mudulia P K 2017 *Appl. Phys. Lett.* **110** 202402
[38] Hayashi M, Kim J, Yamanouchi M and Ohno H 2014 *Phys. Rev. B* **89** 144425
[39] Liu Q B, Zhu L J, Zhang X S, Muller D A and Ralph D C 2022 *Appl. Phys. Rev.* **9** 021402
[40] Yan Z H, Li Z X, Zhu L J, Lin X and Zhu L J 2025 *Chin. Phys. Lett.* **42** 090701
[41] Seki T, Sakuraba Y, Masuda K, Miura A, Tsujikawa M, Uchida K, Kubota T, Miura Y, Shirai M and Takanashi K 2021 *Phys. Rev. B* **103** L020402
[42] Uchida K I, Kikkawa T, Seki T, Oyake T, Shiomi J, Qiu Z, Takanashi K and Saitoh E 2015 *Phys. Rev. B* **92** 094414
[43] Nguyen M H, Ralph D C and Buhrman R A 2016 *Phys. Rev. Lett.* **116** 126601
[44] Liu Q B, Lin X, Shaked A, Nie Z Y, Yu G Q and Zhu L J 2024 *Adv. Mater.* **36** 2406552
[45] Chen T Y, Ou Y X, Tsai T Y, Buhrman R A and Pai C F 2018 *APL Mater.* **6** 121101
[46] Liu Q B and Zhu L J 2025 *Nat. Commun.* **16** 8660
[47] Zhu L J, Liu Q B and Wang X R 2025 *Natl. Sci. Rev.* **12** nwaf240
[48] Liu Q B, Zhu L J and Zhu L J *under review*
[49] Zhu L J and Buhrman R A 2021 *Phys. Rev. Appl.* **15** L031001
[50] Zhang T Y, Zhu L J, Yan Z H and Zhu L J 2025 arXiv:2512.07102
[51] Zhu L J, Ralph D C and Buhrman R A 2019 *Phys. Rev. Lett.* **122** 077201
[52] Zhu L J, Ralph D C and Buhrman R A 2019 *Phys. Rev. B* **99** 180404
[53] Han G L, Lin X, Liu Q B, Gong G W and Zhu L J 2025 *Adv. Funct. Mater.* **36** e23908
[54] Yin X M, Han G L, Gong G W, Kang J, Xiong C M and Zhu L J 2025 *Chin. Phys. Lett.* **42** 110703
[55] Zhu L J, Sobotkiewich K, Ma X, Li X Q, Ralph D C and Buhrman R A 2019 *Adv. Funct. Mater.* **29** 1805822
[56] Zhu L J, Zhu L J, Ma X, Li X Q and Buhrman R A 2022 *Commun. Phys.* **5** 151
[57] Liu Q B, Liu L, Xing G Z and Zhu L J 2024 *Nat. Commun.* **15** 2978
[58] Avci C O, Quindeau A, Pai C F, Mann M, Caretta L, Tang A S, Onbasli M C, Ross C A and Beach G S D 2017 *Nat. Mater.* **16** 309
[59] Zhao Z Y, Jamali M, Smith A K and Wang J P 2015 *Appl. Phys. Lett.* **106** 132404
[60] Yoshimi R, Yasuda K, Tsukazaki A, Takahashi K S, Kawasaki M and Tokura Y 2018 *Sci. Adv.* **4** eaat9989
[61] Liu L, Qin Q, Lin W N, Li C J, Xie Q D, He S K, Shu X Y, Zhou C H, Lim Z S, Yu J H, Lu W L, Li M S, Yan X B, Pennycook S J and Chen J S 2019 *Nat. Nanotechnol.* **14** 939
[62] Huang Q K, Dong Y N, Zhao X N, Wang J, Chen Y X, Bai L H, Dai Y, Dai Y Y, Yan S S and Tian Y F 2020 *Adv. Electron. Mater.* **6** 1900782
[63] Kajale S N, Nguyen T, Hung N T, Li M and Sarkar D 2024 *Sci. Adv.* **10** eadk8669
[64] Zhang Y Y, Ren X L, Liu R Z, Chen Z H, Wu X Z, Pang J, Wang W, Lan G B, Watanabe K, Taniguchi T, Shi Y G, Yu G Q and Shao Q M 2024 *Adv. Mater.* **36** 2406464
[65] Guang Y, Zhang L K, Zhang J W, *et al.* 2023 *Adv. Electron. Mater.* **9** 2200570
[66] Watanabe K, Jinnai B, Fukami S, Sato H and Ohno H 2018 *Nat. Commun.* **9** 663